RSC Advances

PAPER

View Article Online
View Journal | View Issue

Cite this: *RSC Adv.*, 2023, **13**, 9839

Electrochemical ammonia synthesis by reduction of nitrate on Au doped Cu nanowires†

Yuankang Zha, [ab] Min Liu,[a] Jinlu Wang,[a] Jiyu Feng,[a] Daopeng Li,[a] Dongnan Zhao,[a] Shengbo Zhang*[ab] and Tongfei Shi*[ab]

Received 1st February 2023
Accepted 17th March 2023

DOI: 10.1039/d3ra00679d

rsc.li/rsc-advances

Electrochemical nitrate reduction reaction (NO_3^-RR) to synthesize valuable ammonia (NH_3) is considered as a green and appealing alternative to enable an artificial nitrogen cycle. However, as there are other NO_3^-RR pathways present, selectively guiding the reaction pathway towards NH_3 is currently challenged by the lack of efficient catalyst. Here, we demonstrate a novel electrocatalyst for NO_3^-RR consisting of Au doped Cu nanowires on a copper foam (CF) electrode (Au–Cu NWs/CF), which delivers a remarkable NH_3 yield rate of 5336.0 ± 159.2 μg h^{-1} cm^{-2} and an exceptional faradaic efficiency (FE) of 84.1 ± 1.0% at −1.05 V (*vs.* RHE). The ^{15}N isotopic labelling experiments confirm that the yielded NH_3 is indeed from the Au–Cu NWs/CF catalyzed NO_3^-RR process. The XPS analysis and *in situ* infrared spectroscopy (IR) spectroscopy characterization results indicated that the electron transfer between the Cu and Au interface and oxygen vacancy synergistically decreased the reduction reaction barrier and inhibited the generation of hydrogen in the competitive reaction, resulting in a high conversion, selectivity and FE for NO_3^-RR. This work not only develops a powerful strategy for the rational design of robust and efficient catalysts by defect engineering, but also provides new insights for selective nitrate electroreduction to NH_3.

Ammonia (NH_3) is not only an essential chemical and the cornerstone of the large and ever-growing fertilizer industry, but also considered as an important energy storage medium and carbon-free energy carrier.[1–4] Currently, most of the ammonia synthesis in the world is implemented *via* the Haber–Bosch process, which consumes about 5.51 EJ of energy every year (~38 GJ/t_{NH_3}) and emits over 450 million metric tons of CO_2 (~2.9 t_{CO_2}/t_{NH_3}), this is because the process requires substantial driving force and hydrogen gas (*e.g.*, H_2), which is produced from natural gas or coal through steam reforming, accounting for about half of CO_2 emissions in the entire process.[5–8] Nitrogen gas (N_2) from air was identified as one major nitrogen source for this renewable route *via* electrochemical nitrogen reduction reaction (NRR), however, the faradaic efficiency (FE) is greatly hampered by the high dissociation energy of N≡N tripe bond (941 kJ mol^{-1}) and poor solubility of N_2 in electrolytes and the competitive reaction of H_2 evolution.[9–11] While exciting progresses in NRR catalyst development have been made, in many cases it is still challenging to firmly attribute the detected NH_3 to NRR process rather than contaminations due to the extremely low NH_3 production rate (mostly <200 μg h^{-1} $mg_{cat.}^{-1}$).[12,13] Thus, developing a new route for ammonia synthesis under benign conditions is urgently desired.

It is common knowledge that, nitrate pollution in surface water and groundwater is widespread in the world.[14] High concentrations of nitrate in aquatic ecosystems pose a serious threat to ecological balances and human health. To minimize such adverse effects, many approaches including biological denitrification,[15] reverse osmosis,[16] ion exchange,[17] electrodialysis,[18] membrane filtration,[19] electrocatalytic denitrification[20–22] and so on have been adopted to dispose of nitrate contamination to produce clean water, among them, electrocatalytic denitrification driven by "green" electricity generated from renewable resources is the most likely practical alternative, which can overcome these limitations. Compared with the NRR, the nitrate reduction reaction (NO_3^-RR) to NH_3 is not limited by the low solubility of N_2 in water environment and its thermodynamically more favourable because of lower dissociation energy of N=O bond (204 kJ mol^{-1}) than the N≡N tripe bond (941 kJ mol^{-1}).[23,24] Therefore, it is an frontier field that needs in-depth study.

Herein, we utilized a facile three-step method to fabricate the Au doped Cu nanowires on a copper foam (CF) (denoted as Au–Cu NWs/CF) electrode for the selective nitrate electroreduction to ammonia. The Au–Cu NWs/CF sample exhibited an exceptional performance with the NH_3 yield rate of 5336.0 ± 159.2 μg h^{-1} cm^{-2} and the FE of 84.1 ± 1.0% at −1.05 V (*vs.* RHE) for the electrocatalytic NO_3^-RR under

[a]*Key Laboratory of Materials Physics, Institute of Solid State Physics, HFIPS, Chinese Academy of Sciences, Hefei 230031, China. E-mail: tfshi@issp.ac.cn; shbzhang@issp.ac.cn*

[b]*University of Science and Technology of China, Hefei 230026, China*

† Electronic supplementary information (ESI) available: Details of experimental process, calibration curves and electrochemical measurement results. See DOI: https://doi.org/10.1039/d3ra00679d

neutral conditions. ^{15}N isotopic labelling experiments were performed to confirm the origin of ammonia, which was quantified by both ^{1}H nuclear magnetic resonance (NMR) spectra and colorimetric methods. The XPS analysis and *in situ* infrared spectroscopy (IR) spectroscopy characterization results indicated that the oxygen vacancies in Au–Cu NWs/CF can weaken the N–O bonding,[25] moreover, the electron transfer between Cu and Au interface could inhibit the competitive reaction of the hydrogen evolution reaction (HER),[11] resulting in high NH_3 yield rate and FE of NO_3^-RR.

Fig. 1a shows the schematic illustration of the growth of the Au doped Cu nanowires on a copper foam electrode. As illustrated in Fig. 1a, Au–Cu NWs/CF can be prepared by a three-step method. In the first step, the $Cu(OH)_2$ NWs/CF was prepared *via* a facile wet-chemical oxidation method. Subsequently, NWs/CF was directly immersed into 10 mM $HAuCl_4 \cdot 3H_2O$ solution for 12 h, dried at 60 °C under vacuum for 4 h, the Au–$Cu(OH)_2$ NWs/CF was annealed under Ar atmosphere to obtain Au–CuO NWs/CF. Finally, the Au–Cu NWs/CF was obtained by *in situ* electrochemical reduction of the resultant Au–CuO NWs/CF. The scanning electron microscopy (SEM) images of CF (Fig. 1b) and Au–Cu NWs/CF (Fig. 1c) demonstrate that the nanowires have been successfully generated on CF. After cation exchange reaction with Au precursor and subsequent thermal treatment and electrochemical reduction, the morphology of nanowires was largely maintained on the Au–Cu NWs/CF with the diameters of ~100 nm (Fig. 1c). Fig. 1d shows the X-ray diffraction (XRD) patterns of CF and Au–Cu NWs/CF samples. As shown, similar diffraction peaks at $2\theta = 43.3°$, 50.4° and 74.1° can be observed for these two samples, corresponding to (111), (200) and (220) plane of metallic Cu (JCPDS no. 04-0836), respectively.[26–28] While besides of typical diffraction peaks of metallic Cu, the Au–Cu NWs/CF sample also displays the weak characteristic peaks of Au nanoparticles at 2θ = 38.2°, 44.3°, 64.6° and 77.5°, suggesting the formation of fcc Au phase on Cu nanowires with low loading content.[29] The actual loading of Au was calculated to be 5.6 wt% by inductively couple plasma atomic emission spectroscopy (ICP-AES). High-resolution TEM (HR-TEM, Fig. 1e) images show the lattice fringes of 0.24 and 0.27 nm, corresponding to the (111) and (200) planes of Cu, respectively, in good accord with the XRD results.[27,28] In addition, the corresponding element mapping analysis of Au–Cu NWs/CF reveals that Au was homogeneously dispersed over the whole Cu foam (Fig. 1f).

The X-ray photoelectron spectroscopy (XPS) measurement was performed to investigate the surface composition and valence state of Au–Cu NWs/CF. For comparison, we also performed the XPS characterization of CF sample. The XPS survey spectra and high-resolution XPS spectra of Au 4f verified the existence of doped Au in the Au–Cu NWs/CF (Fig. 2a and b). The high-resolution XPS spectra of Cu 2p in bare CF substrate is shown in Fig. 2c, where peaks of Cu $2p_{3/2}$ and Cu $2p_{1/2}$ appear at 932.5 and 952.3 eV.[26–28] The two characteristic peaks confirms the presence of Cu^0/Cu^{1+}.[26–28] Note that after Au doping, the binding energy of Cu $2p_{3/2}$ and Cu $2p_{1/2}$ shifted by 0.5 eV and 0.4 eV towards the lower binding energy of 932.0 and 951.9 eV in Au–Cu NWs/CF (Fig. 2c), due to the transfer of electrons

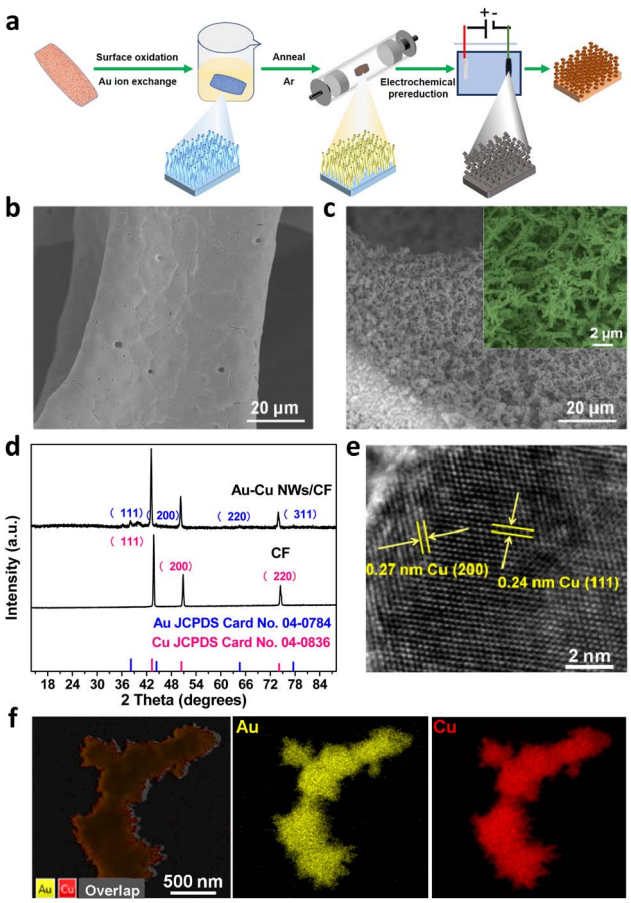

Fig. 1 (a) Schematic illustration and corresponding structure of products. SEM images of (b) bare CF substrate and (c) Au–Cu NWs/CF. (d) XRD patterns for CF and Au–Cu NWs/CF. (e) HR-TEM image of Au–Cu NWs/CF. (f) EDS images of Au–Cu NWs/CF.

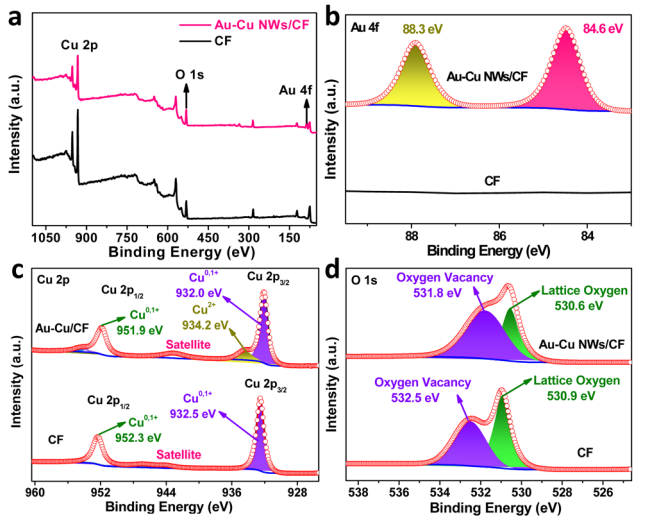

Fig. 2 (a) Surface survey XPS spectra of Au–Cu NWs/CF and CF samples. High-resolution XPS spectra of (b) Au 4f, (c) Cu 2p and (d) O 1s in Au–Cu NWs/CF and CF samples.

between Cu and Au *via* chemical binding, which led to an increase in charge density and is conducive to electrocatalysis.[27,28] Additionally, the new peak at binding energy of 934.2 eV was attributed to Cu^{2+} in Au–Cu NWs/CF. Based on previous reports,[27,28] we further used Auger Cu LMM spectra to confirm the coexistence of Cu^0 and Cu^{1+}. It can be clearly observed in the Fig. S1† (ESI) that the Auger kinetic energy peak is wide and asymmetric in the range of 906 eV to 924 eV. The two asymmetric peaks with centers located at the position around 916.5 and 918.7 eV, 916.1 eV and 918.4 eV can be assigned to Cu^{1+} and Cu^0 in the CF and Au–Cu NWs/CF, respectively.[27,28] In the O 1s XPS spectra (Fig. 2d), 530.9 and 532.5 eV, 530.6 eV and 531.8 eV correspond to lattice oxygen and oxygen vacancy in the CF and Au–Cu NWs/CF, respectively.[26] The significantly increased oxygen vacancy after doping is favourable for weakening the N–O bond and inhibiting the formation of by-products in the electrocatalytic nitrate reduction reaction, thereby improving the selectivity of ammonia.[25]

We evaluated the NO_3^-RR performance of the as-fabricated Au–Cu NWs/CF catalysts in a 0.1 M Na_2SO_4 + 10.0 mM KNO_3 solution (pH = 5.6) using a three-electrode configured two-compartment cell. In all experiments, the Au–Cu NWs/CF catalyst was used as working electrode, Ag/AgCl (saturated KCl solution) and Pt mesh were used as the reference electrode and counter electrode, respectively. Colorimetric methods were adopted determine the concentration of NO_3^-, NO_2^- and NH_4^+ (Fig. S2, S3 and S4, ESI†). The liner sweep voltammetry (LSV) curves of Au–Cu NWs/CF electrocatalysts was conducted in 0.1 M Na_2SO_4 electrolytes with and without 10.0 mM KNO_3. As shown in Fig. 3a, the current density increased obviously with the present of KNO_3, suggesting that NO_3^- in solution participated in the reduction reactions. Note that the LSV of Au–Cu NWs/CF tested in the presence of NO_3^- exhibits a remarkable reduction peak at −0.6 V (*vs.* RHE), which may be due to the electrochemical reduction of NO_3^-. Chronoamperometry (CA) measurements of Au–Cu NWs/CF were conducted at different potentials for 2 h with continuous argon gas (Ar) bubbling. Fig. S5a† (ESI) shows the chronoamperometry curves at each given potential for 2 h electrolysis from −0.7 V to −1.1 V (*vs.* RHE). The concentration of NH_3 product was measured using indophenol blue method (Fig. S5b, ESI†). The calculated NH_3 yield rates and FEs based on three repeated experiments are given in Fig. 3b. It is worth noting that the Au–Cu NWs/CF achieved the highest NH_3 yield rate (R_{NH_3}) of 5336.0 ± 159.2 μg h^{-1} cm^{-2} and the FE of 84.1 ± 1.0% at −1.05 V (*vs.* RHE). The selectivity of NH_3 (S_{NH_3}) and R_{NH_3} show the same trend with the increase of potential, and highest S_{NH_3} was 90.6 ± 3.2% (Fig. 3c). In addition, the conversion of nitrate increases slowly with the increase of potential, and 100% conversion can be achieved at −0.95 V (*vs.* RHE) (Fig. 3d). When the potential further increased to −1.1 V (*vs.* RHE), the R_{NH_3} and S_{NH_3} decreased due to the competitive hydrogen evolution reaction (HER).[30] Although the electrodynamic potential of NO_3^- to NO_2^- is higher than that of NO_3^- to NH_3, NO_2^- is easily detected an main by-product of NO_3^-RR.[31] As shown in Fig. S6† (ESI), few NO_2^- is detected after electrocataytic reduction at −1.05 V (*vs.* RHE), further demonstrating the high selective reduction of nitrate to NH_3. We also tested R_{NH_3} and FE of bare CF with 0.1 M Na_2SO_4 + 10.0 mM KNO_3 solution at −1.05 V (*vs.* RHE) to exclude the influence of substrate. As shown in Fig. S7† (ESI), the highest R_{NH_3} and FE for bare CF were 1777.7 μg h^{-1} cm^{-2} and the FE of 49.9%, much lower than Au–Cu NWs/CF. The corresponding equivalent circuit diagrams of bare CF and Au–Cu NWs/CF are shown in Fig. S8† (ESI). The much lower ohmic resistances (R_s) and charge-transfer resistance (R_{ct}) from Au–Cu NWs/CF confirms its high electrical conductivity, which could be an important attribute for the achieved high R_{NH_3} and FE.

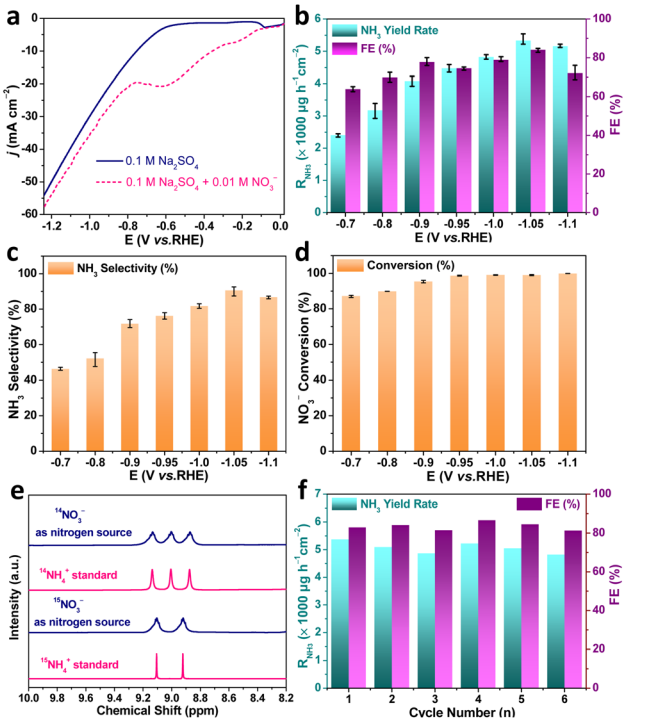

Fig. 3 (a) LSV curves of Au–Cu NWs/CF catalyst in 0.1 M Na_2SO_4 and 0.1 M Na_2SO_4 + 10.0 mM KNO_3 solution. (b) NH_3 yield rate and faradaic efficiency of Au–Cu NWs/CF catalyst obtained at different potentials for 2 h NO_3^-RR measurement. (c) NH_3 selectivity and (d) NO_3^- conversion of Au–Cu NWs/CF catalyst obtained at different potentials. (e) ^{1}H NMR spectra of Au–Cu NWs/CF catalyst using $^{14}NO_3^-$/$^{15}NO_3^-$ as nitrogen source for NO_3^-RR and standards $(^{14}NH_4)_2SO_4$/$(^{15}NH_4)_2SO_4$. (f) Recycling tests for Au–Cu NWs/CF catalyst during NO_3^-RR at −1.05 V (*vs.* RHE).

^{15}N isotope labeling with ^{1}H nuclear magnetic resonance (NMR) is usually required in NO_3^-RR experiments to confirm that the detected NH_3 indeed originates from the electrochemical nitrate reduction to rule out contaminations. We carried out chronoamperometry measurement at −1.05 (V *vs.* RHE) for 2 h in the electrolyte with $K^{15}NO_3$ and $K^{14}NO_3$ as N source, respectively. As shown in Fig. 3e, when the electrolysis was carried out in solution with $K^{14}NO_3$, the ^{1}H NMR spectra of the obtained products displayed typical peaks of $^{14}NH_4^+$. In contrast, when the $K^{15}NO_3$ was used as nitrogen source, the ^{1}H NMR spectra showed typical double peaks of $^{15}NH_4^+$. Such results indicated that the produced NH_3 was entirely derived from the nitrate in the electrolyte, rather than from the contaminations. Meanwhile, the electrolyte without nitrate

addition is also tested. The electrochemical measurement in blank 0.1 M Na_2SO_4 electrolyte produced ignorable NH_3 (Fig. S9, ESI†), further confirming that the produced NH_3 orginated from nitrate electroreduction. The durability of the Au–Cu NWs/CF electrocatalyst for NO_3^-RR was subsequently assessed by consecutive recycling electrolysis at −1.05 V (*vs.* RHE), no noticeable decay in the cathodic current density and UV-vis absorptions (Fig. S10, ESI†). As shown in Fig. 3f, the R_{NH_3} and FE are stable after 6 consecutive recycling tests, indicating the good durability of Au–Cu NWs/CF.

After electrolysis, the high-resolution Au 4f and Cu LMM XPS spectra were carried out to analyze the electronic properties of Au–Cu NWs/CF before and after NO_3^-RR measurement (Fig. S11, ESI†). Interestingly, after NO_3^-RR, the Au $4f_{7/2}$ shifted slightly to a lower binding energy by 0.2 eV after electrolysis (Fig. S11a, ESI†). Similarly, the Auger peak of Cu^{2+} shifted to a lower binding energy by 0.3 eV, while the Auger peaks of Cu^0 and Cu^{1+} shifted to the higher binding energy by 0.2 eV and 0.3 eV after electrolysis (Fig. S11c, ESI†), indicating the existence of charge transfer between Au, Cu^{2+} and $Cu^{0,+1}$ during NO_3^-RR process. Inaddition, the oxygen defect increased significantly after electrolysis (Fig. S11d, ESI†). In a word, the high electronic density of Cu^0 and oxygen vacancy decreased the reduction reaction barrier and inhibited the generation of hydrogen in the competitive reaction, resulting in a high conversion, selectivity and FE of Au–Cu NWs/CF for NO_3^-RR.[31,32]

To gain a deeper understanding of the NO_3^-RR mechanism over Au–Cu NWs/CF catalysts, we utilized *in situ* infrared spectroscopy (IR) spectroscopy characterization to detect intermediates and monitor the reaction. Fig. 4a display the *in situ* IR spectra of Au–Cu NWs/CF under various potentials. As shown, without the applied potential, there is no any infrared peak in the *in situ* IR spectra. In the investigated potential range from −0.7 to −1.1 V (*vs.* RHE), the new infrared bands at ~1541 cm^{-1} was assigned to the $-NO_x$ intermediates.[33,34] In addition, the bending mode of $-NH_2$ is also found at ~1457 cm^{-1}.[34,35] Clearly, as the applied potential increased, the peak intensity of $-NO_x$ intermediates and $-NH_2$ gradually increased (Fig. 4a). Fig. 4b shows the *in situ* IR measurements for the NO_3^-RR at −1.05 V (*vs.* RHE). The IR intensity of the peaks at around 1457 cm^{-1} and 1541 cm^{-1}, corresponding to $-NH_2$ and $-NO_x$ intermediates is increased obviously from 4 to 36 min, implying that the NO_3^-RR takes place gradually with reaction time under the given electrocatalytic conditions. Evidenced by the *in situ* IR results, the NH_3 synthesis by NO_3^-RR is successfully achievable (Fig. S12, ESI†), supportable for the electrocatalytic experimental results aforementioned.

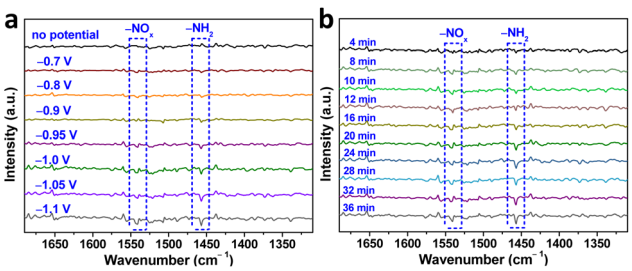

Fig. 4 (a) *In situ* IR spectroscopy measurements under various potentials for Au–Cu NWs/CF in 1.0 M Na_2SO_4 + 10.0 mM KNO_3 electrolyte. (b) *In situ* IR spectroscopy measurements of Au–Cu NWs/CF in 1.0 M Na_2SO_4 + 10.0 mM KNO_3 electrolyte at −1.05 V (*vs.* RHE) for NO_3^-RR.

In conclusion, Au doped Cu nanowires on a copper foam electrode was synthesized *via* a facile three-step method, which further generated the oxygen vacancies in Au–Cu NWs/CF can weaken the N–O bonding, moreover, the electron transfer between Cu and Au interface could inhibit the competitive reaction, resulting in high conversion, selectivity and FE of Au–Cu NWs/CF for NO_3^-RR. The Au–Cu NWs/CF exhibited significantly enhanced NO_3^-RR activity with an NH_3 yield rate of 5336.0 ± 159.2 μg h^{-1} cm^{-2} and the FE of 84.1 ± 1.0% at −1.05 V (*vs.* RHE) in neutral electrolyte. The *in situ* IR spectroscopy measurements confirm the successful realization of NH_3 synthesis by NO_3^-RR over Au–Cu NWs/CF. Our work would be helpful to design and develop high-efficiency NO_3^-RR electrocatalysts for ambient electrosynthesis of ammonia.

Conflicts of interest

There are no conflicts to declare.

Acknowledgements

This work was financially supported by Anhui Provincial Natural Science Foundation (Grant No. 2108085QB60 and 2108085QB61), CASHIPS Director's Fund (Grant No. YZJJ2021QN18 and YZJJ2021QN21), China Postdoctoral Science Foundation (Grant No. 2020M682057), Special Research Assistant Program, Chinese Academy of Sciences.

Notes and references

1 S. L. Foster, S. I. P. Bakovic, R. D. Duda, S. Maheshwari, R. D. Milton, S. D. Minteer, M. J. Janik, J. N. Renner and L. F. Greenlee, Catalysts for nitrogen reduction to ammonia, *Nat. Catal.*, 2018, **1**, 490.

2 Y. Ashida, K. Arashiba, K. Nakajima and Y. Nishibayashi, Molybdenumcatalysed ammonia production with samarium diiodide and alcohols or water, *Nature*, 2019, **568**, 536.

3 C. Tang and S.-Z. Qiao, How to explore ambient electrocatalytic nitrogen reduction reliably and insightfully, *Chem. Soc. Rev.*, 2019, **48**, 3166.

4 W. He, J. Zhang, S. Dieckhöfer, S. Varhade, A. C. Brix, A. Lielpetere, S. Seisel, J. R. Junqueira and W. Schuhmann, Splicing the active phases of copper/cobalt-based catalysts achieves high-rate tandem electroreduction of nitrate to ammonia, *Nat. Commun.*, 2022, **13**, 1.

5 J. Lim, C. A. Fernández, S. W. Lee and M. C. Hatzell, Ammonia and nitric acid demands for fertilizer use in 2050, *ACS Energy Lett.*, 2021, **6**, 3676.

6 H. Liu, X. Lang, C. Zhu, J. Timoshenko, M. Rüscher, L. Bai, N. Guijarro, H. Yin, Y. Peng and J. Li, Copper-supported

Rhodium cluster and single-atom catalysts, *Angew. Chem., Int. Ed.*, 2022, e202202556.
7 X. Fu, X. Zhao, X. Hu, K. He, Y. Yu, T. Li, Q. Tu, X. Qian, Q. Yue and M. R. Wasielewski, Alternative route for electrochemical ammonia synthesis by reduction of nitrateon copper nanosheets, *Appl. Mater. Today*, 2020, **19**, 100620.
8 C. Liu, K. K. Sakimoto, B. C. Colón, P. A. Silver and D. G. Nocera, Ambient nitrogen reduction cycle using a hybrid inorganic–biological system, *Proc. Natl. Acad. Sci. U. S. A.*, 2017, **114**, 6450.
9 H. Jia, A. Du, H. Zhang, J. Yang, R. Jiang, J. Wang and C.-y. Zhang, Site-selective growth of crystalline ceria with oxygen vacancies on gold nanocrystals for near-infrared nitrogen photofixation, *J. Am. Chem. Soc.*, 2019, **141**, 5083.
10 M.-A. Légaré, G. Bélanger-Chabot, R. D. Dewhurst, E. Welz, I. Krummenacher, B. Engels and H. Braunschweig, Nitrogen fixation and reduction at boron, *Science*, 2018, **359**, 896.
11 Y. Yu, C. Wang, Y. Yu, Y. Wang and B. Zhang, Promoting selective electroreduction of nitrates to ammonia over electron-deficient Co modulated by rectifying Schottky contacts, *Sci. China: Chem.*, 2020, **63**, 1469.
12 S. Z. Andersen, V. Čolić, S. Yang, J. A. Schwalbe, A. C. Nielander, J. M. McEnaney, K. Enemark-Rasmussen, J. G. Baker, A. R. Singh and B. A. Rohr, A rigorous electrochemical ammonia synthesis protocol with quantitative isotope measurements, *Nature*, 2019, **570**, 504.
13 Z.-Y. Wu, M. Karamad, X. Yong, Q. Huang, D. A. Cullen, P. Zhu, C. Xia, Q. Xiao, M. Shakouri and F.-Y. Chen, Electrochemical ammonia synthesis via nitrate reduction on Fe single atom catalyst, *Nat. Commun.*, 2021, **12**, 1.
14 T. Zhu, Q. Chen, P. Liao, W. Duan, S. Liang, Z. Yan and C. Feng, Single-atom Cu catalysts for enhanced electrocatalytic nitrate reduction with significant alleviation of nitrite production, *Small*, 2020, **16**, 2004526.
15 P. Clauwaert, K. Rabaey, P. Aelterman, L. De Schamphelaire, T. H. Pham, P. Boeckx, N. Boon and W. Verstraete, Biological denitrification in microbial fuel cells, *Environ. Sci. Technol.*, 2007, **41**, 3354.
16 R. Epsztein, O. Nir, O. Lahav and M. Green, Selective nitrate removal from groundwater using a hybrid nanofiltration–reverse osmosis filtration scheme, *Chem. Eng. J.*, 2015, **279**, 372.
17 A. D. Fonseca, J. G. Crespo, J. S. Almeida and M. A. Reis, Drinking water denitrification using a novel ion-exchange membrane bioreactor, *Environ. Sci. Technol.*, 2000, **34**, 1557.
18 F. D. Belkada, O. Kitous, N. Drouiche, S. Aoudj, O. Bouchelaghem, N. Abdi, H. Grib and N. Mameri, Electrodialysis for fluoride and nitrate removal from synthesized photovoltaic industry wastewater, *Sep. Purif. Technol.*, 2018, **204**, 108.
19 R. Mukherjee and S. De, Adsorptive removal of nitrate from aqueous solution by polyacrylonitrile–alumina nanoparticle mixed matrix hollow-fiber membrane, *J. Membr. Sci.*, 2014, **466**, 281.
20 S. Ye, Z. Chen, G. Zhang, W. Chen, C. Peng, X. Yang, L. Zheng, Y. Li, X. Ren and H. Cao, Elucidating the activity, mechanism and application of selective electrosynthesis of ammonia from nitrate on cobalt phosphide, *Energy Environ. Sci.*, 2022, **15**, 760.
21 N. C. Kani, J. A. Gauthier, A. Prajapati, J. Edgington, I. Bordawekar, W. Shields, M. Shields, L. C. Seitz, A. R. Singh and M. R. Singh, Solar-driven electrochemical synthesis of ammonia using nitrate with 11% solar-to-fuel efficiency at ambient conditions, *Energy Environ. Sci.*, 2021, **14**, 6349.
22 G. Wen, J. Liang, Q. Liu, T. Li, X. An, F. Zhang, A. A. Alshehri, K. A. Alzahrani, Y. Luo and Q. Kong, Ambient ammonia production via electrocatalytic nitrite reduction catalyzed by a CoP nanoarray, *Nano Res.*, 2022, **15**, 972.
23 Z. Gong, W. Zhong, Z. He, Q. Liu, H. Chen, D. Zhou, N. Zhang, X. Kang and Y. Chen, Regulating surface oxygen species on copper (I) oxides via plasma treatment for effective reduction of nitrate to ammonia, *Appl. Catal., B*, 2022, **305**, 121021.
24 L. Li, C. Tang, X. Cui, Y. Zheng, X. Wang, H. Xu, S. Zhang, T. Shao, K. Davey and S. Z. Qiao, Efficient nitrogen fixation to ammonia through integration of plasma oxidation with electrocatalytic reduction, *Angew. Chem., Int. Ed.*, 2021, **60**, 14131.
25 R. Jia, Y. Wang, C. Wang, Y. Ling, Y. Yu and B. Zhang, Boosting selective nitrate electroreduction to ammonium by constructing oxygen vacancies in TiO_2, *ACS Catal.*, 2020, **10**, 3533.
26 J. Wang, S. Zhang, C. Wang, K. Li, Y. Zha, M. Liu, H. Zhang and T. Shi, Ambient ammonia production via electrocatalytic nitrate reduction catalyzed by flower-like $CuCo_2O_4$ electrocatalyst, *Inorg. Chem. Front.*, 2022, **9**, 2374.
27 S. Zhang, C. Zhao, Y. Liu, W. Li, J. Wang, G. Wang, Y. Zhang, H. Zhang and H. Zhao, Cu doping in CeO_2 to form multiple oxygen vacancies for dramatically enhanced ambient N_2 reduction performance, *Chem. Commun.*, 2019, **55**, 2952.
28 Y. Wang, Z. Chen, P. Han, Y. Du, Z. Gu, X. Xu and G. Zheng, Single-atomic Cu with multiple oxygen vacancies on ceria for electrocatalytic CO_2 reduction to CH_4, *ACS Catal.*, 2018, **8**, 7113.
29 Y. Chen, Z. Fan, Z. Luo, X. Liu, Z. Lai, B. Li, Y. Zong, L. Gu and H. Zhang, High-yield synthesis of crystal-phase-heterostructured 4H/fcc Au@Pd core–shell nanorods for electrocatalytic ethanol oxidation, *Adv. Mater.*, 2017, **29**, 1701331.
30 T. Oshikiri, K. Ueno and H. Misawa, Selective dinitrogen conversion to ammonia using water and visible light through plasmon-induced charge separation, *Angew. Chem., Int. Ed.*, 2016, **55**, 3942.
31 Y. Wang, W. Zhou, R. Jia, Y. Yu and B. Zhang, Unveiling the activity origin of a copper-based electrocatalyst for selective nitrate reduction to ammonia, *Angew. Chem., Int. Ed.*, 2020, **59**, 5350.
32 J. Geng, S. Ji, H. Xu, C. Zhao, S. Zhang and H. Zhang, Electrochemical reduction of nitrate to ammonia in

a fluidized electrocatalysis system with oxygen vacancy-rich CuO_x nanoparticles, *Inorg. Chem. Front.*, 2021, **8**, 5209.
33 L. Chen, J. Li and M. Ge, DRIFT study on cerium–tungsten/titiania catalyst for selective catalytic reduction of NOx with NH3, *Environ. Sci. Technol.*, 2010, **44**, 9590.
34 Z. Song, Y. Liu, Y. Zhong, Q. Guo, J. Zeng and Z. Geng, Efficient electroreduction of nitrate into ammonia at ultralow concentrations via an enrichment effect, *Adv. Mater.*, 2022, **34**, 2204306.
35 E. Pérez-Gallent, M. C. Figueiredo, I. Katsounaros and M. T. Koper, Electrocatalytic reduction of nitrate on copper single crystals in acidic and alkaline solutions, *Electrochim. Acta*, 2017, **227**, 77.